Early stages of spinodal decomposition in Fe–Cr resolved by *in-situ* small-angle neutron scattering

M. Hörnqvist,[1,a)] M. Thuvander,[1] A. Steuwer,[2,3] S. King,[4] J. Odqvist,[5] and P. Hedström[5]

[1]*Department of Applied Physics, Chalmers University of Technology, Fysikgränd 3, S-412 96 Gothenburg, Sweden*
[2]*MAX IV Laboratory, Lund University, S-221 00 Lund, Sweden*
[3]*Nelson Mandela Metropolitan University, Gardham Ave., Port Elizabeth 6031, South Africa*
[4]*ISIS Facility, Rutherford Appleton Laboratory, Chilton, OX11 0QX Didcot, United Kingdom*
[5]*Materials Science and Engineering, KTH Royal Institute of Technology, Brinellvägen 23, S-100 44 Stockholm, Sweden*

In-situ, time-resolved small-angle neutron scattering (SANS) investigations of the early stages of the spinodal decomposition process in Fe–35Cr were performed at 773 and 798 K. The kinetics of the decomposition, both in terms of characteristic distance and peak intensity, followed a power-law behaviour from the start of the heat treatment ($a' = 0.10$–0.11 and $a'' = 0.67$–0.86). Furthermore, the method allows tracking of the high–Q slope, which is a sensitive measure of the early stages of decomposition. *Ex-situ* SANS and atom probe tomography were used to verify the results from the *in-situ* investigations. Finally, the *in-situ* measurement of the evolution of the characteristic distance at 773 K was compared with the predictions from the Cahn-Hilliard-Cook model, which showed good agreement with the experimental data ($a' = 0.12$–0.20 depending on the assumed mobility). © 2015 AIP Publishing LLC. [http://dx.doi.org/10.1063/1.4908250]

Spinodal decomposition of the bcc phase in Fe–Cr alloys into an Fe-rich and a Cr-rich phase is a widely studied phenomenon. The reason is two-fold: First, the system is the basis of the industrially important stainless steel family, where the decomposition of the bcc phase in ferritic, duplex and to some extent martensitic and δ-ferrite containing austenitic grades, is partially responsible for degradation of the mechanical properties over time during elevated temperature exposure in service. Second, the Fe–Cr system is ideal to study the fundamentals of the spinodal decomposition process, since it offers a combination of a wide miscibility gap, a rather wide temperature range where the kinetics of the decomposition is suitable for practical measurements and minor coherency strains.

The decomposition process in Fe–Cr is typically investigated by transmission electron microscopy (TEM),[1] Mössbauer spectroscopy,[2,3] atom probe tomography (APT),[4,5] or small-angle neutron scattering (SANS).[6–8] While each technique has its specific advantages, only SANS readily offers the possibility to perform time-resolved *in-situ* measurements at elevated temperatures. However, so far only very few investigations have taken advantage of this possibility of direct continuous tracking of the kinetics without any specimen-to-specimen variations in composition, starting structure, or isothermal temperature. For the Fe–Cr(–Ni) system, there are only two readily available reports of *in-situ* SANS experiments,[9,10] although other systems have been investigated more recently, e.g., Fe–Co–Mo.[11] In Refs. 9 and 10, acquisition times of several hours were used, which resulted in poor temporal resolution. Furusaka *et al.*[12] used *in-situ* SANS to investigate the critical scattering of Fe–Cr alloys in the vicinity of the Curie temperature, but the subsequent investigations of aged alloys were performed *ex-situ*.

The existence and location of the spinodal in the binary Fe–Cr system are today rather well described, both from thermodynamic modelling and experiments (see, e.g., Ref. 13, and references therein). Direct observations from three dimensional APT investigations have also demonstrated the transition of the phase separation mechanism from nucleation-and-growth to spinodal decomposition in the composition range of 25–35% Cr at 773 K.[13] Whereas the spinodal nature of the decomposition process have been questioned for similar systems, e.g., Fe–Cr–Co,[14] based on the development of the SANS invariant during ageing, similar studies of the Fe–Cr binary system show no such indications.[6]

During the spinodal decomposition, a characteristic interconnected structure with nano-scale modulations of the composition forms. This results in the appearance of an interference peak in the structure factor at scattering vector Q_p ($Q = 4\pi \sin \theta / \lambda$, where λ is the neutron wavelength and θ is half the scattering angle) corresponding to a characteristic length scale $\Lambda = 2\pi / Q_p$, usually interpreted as the modulation wavelength of the decomposed structure. Typically, Q_p follows a power-law relationship with annealing time, $Q_p \propto t^{-a'}$. Similarly, the maximum scattered intensity follows $I_p = d\Sigma/d\Omega(Q_p) \propto t^{a''}$, where $d\Sigma/d\Omega$ is the macroscopic scattering cross-section (from hereon, I is used instead of $d\Sigma/d\Omega$ for brevity). Such behaviour is in general agreement with both theoretical predictions (where $a' = 1/6$ and $a'' = 1/2$)[15] and Monte-Carlo simulations (yielding $a' = 0.2$–0.28 and $a'' = 0.65$–0.74).[16,17]

In the present letter, we present a time-resolved *in-situ* SANS investigation of spinodal decomposition in the Fe–Cr system with sufficient temporal resolution to study the early stages of the process. The aim is to investigate the short-time kinetics of spinodal decomposition in the relevant stages where embrittlement often occurs.[18] Furthermore, the *in-situ*

a)magnus.hornqvist@chalmers.se

data are used to make comparisons with theoretical predictions from the Cahn-Hilliard-Cook (CHC) model.[7,19]

The binary Fe–Cr alloy was produced by vacuum arc melting (see Ref. 13 for more details on material preparation), followed by solution treatment at 1373 K for 2 h under pure argon and a final quench in brine. The final alloy composition (in wt. %) was Fe–36.1Cr–0.27Si–0.09Mn–0.02Ni–0.008N–0.005P–0.005C. This composition is within the spinodal and has been shown previously to result in the characteristic interconnected structure during ageing at the intended temperatures.[13] The material was cut into approximately 1.5 mm thick pieces with a 10×10 mm square cross-section and subsequently ground and polished to remove surface oxides.

SANS data were obtained on the LOQ small-angle diffractometer at the ISIS Pulsed Neutron Source (STFC Rutherford Appleton Laboratory, Didcot, UK).[20] This is a fixed-geometry white beam time-of-flight instrument which utilizes neutrons with wavelengths between 0.2 and 1.0 nm. Data are simultaneously recorded on two, two-dimensional, position-sensitive neutron detectors, to provide a simultaneous Q-range of 0.06–14 nm^{-1}.

A vacuum furnace was used to heat the specimens during *in-situ* measurements. The specimens were mounted in pockets made from vanadium sheet (with negligible coherent scattering cross-section), and a thermocouple was placed close to the specimen to monitor and control the temperature. During the tests, the specimens were heated as rapidly as possible without causing temperature overshoots, giving typical heat-up times of around 20 min, and the measurements were started immediately upon reaching the desired temperature (773 and 798 K). Measurements lasting 15 min were performed back-to-back for a total time of 10 h, i.e., each data set consisted of data time-averaged over 15 min. The raw scattering data were corrected for detector efficiencies, sample transmission, and background scattering (including contribution from the Vanadium pocket) and converted to macroscopic scattering cross-section using the MantidPlot software,[21] version 3.1.1. The data were placed on an absolute scale (cm^{-1}) using the scattering from a standard sample (a solid blend of hydrogenous and predeuterated polystyrene) in accordance with established procedures.[22]

In the present investigation, no external magnetic field was applied due to the configuration of the furnace. Therefore, the recorded scattering is the sum of the nuclear and magnetic contributions, where the latter is related to both magnetic domain structure and spin-misalignment, see, e.g., Ref. 23. If not accounted for, the magnetic contribution can affect the accuracy of the data analysis, since the structure factors for nuclear and magnetic scattering are not necessarily the same, and the length scales can overlap. Previous studies without external magnetisation have argued that the nuclear and magnetic contributions are proportional, based on separation of the cross-sections in applied magnetic fields.[7,9,10] This does not ensure proportionality in the absence of magnetic saturation, since the applied magnetic field removes the spatial distribution of magnetic moments from spin-misalignment. However, Isalgué *et al.*[24] showed that the structure factor of a decomposed Fe–28Cr–2Mo–4Ni–Nb alloy obtained with and without an

applied magnetic field (5 kOe) were proportional above $Q > 0.3$ nm^{-1}. As the magnetic field is expected to remove or at least significantly reduce the contribution also from spin-misalignment, the measured proportionality between scattering with and without external magnetisation suggests that the contribution from spin-misalignment is negligible. The increased scattering at lower Q in the absence of an applied magnetic field was attributed to the presence of magnetic domains. Since the length scale is much larger than the expected modulation wavelength of the decomposed structure, it should not interfere with the present measurements. Although the study by Isalgué *et al.*[24] was performed at room temperature (RT), the good agreement between *in-situ* and *ex-situ* data obtained herein suggests that the assumption holds also at elevated temperatures. Furthermore, the present results are validated against APT data, which are independent of the distribution of magnetic moments.

In order to isolate the scattering contribution from the spinodal decomposition process, the following procedure was applied to each data set. A polynomial was fitted to the $\log(I)$ vs. $\log(Q)$ curve, excluding the region where scattering from the decomposition process was observed, in order to separate the background signal (I_b). Whereas ideally the scattering curve obtained directly after heating would be used to define the background, the procedure above was necessary since the background was not constant during the experiments. By dividing the scattered signal by the background, a normalised signal ($I_n = I/I_b$) was obtained. This normalised signal was fitted with a Gaussian function, I_{nG}, with $\log(Q)$ as argument, and the signal from the spinodal decomposition was calculated as $I_{sd} = I_b(I_{nG} - 1)$. The procedure is outlined graphically in Fig. 1. The reason for using a Gaussian fit of I_n rather than just subtracting the fitted background from the total signal was two-fold. First, using the normalised signal proved to be more sensitive in the early stages of the separation. Second, the procedure ensures that there are no spurious negative data points arising from the subtraction. The values of
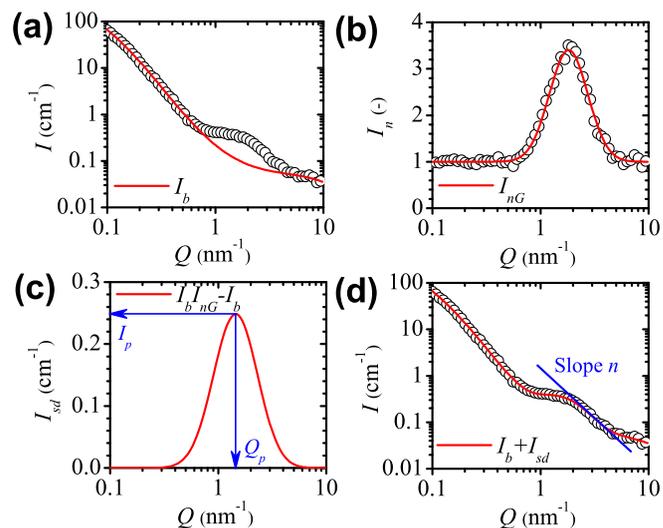

FIG. 1. (a) Fitting of background, I_b. (b) Fitting of a Gaussian function, I_{nG}, to the normalised signal, $I_n = I/I_b$. (c) Calculation of scattered signal from spinodal decomposition, $I_{sd} = I_b(I_{nG} - 1)$. Arrows show the identification of Q_p and I_p. (d) Total signal, $I = I_b + I_{sd}$, including an illustration of the high-Q slope, n.

interest, Q_p and I_p, were then extracted from the obtained Q–I_{sd} curves, as shown in Fig. 1(c).

For comparison, two quenched specimens were also subjected to *ex-situ* heat treatments at 773 K for 1 and 10 h and investigated by *ex-situ* SANS at room temperature, employing otherwise the same experimental settings (apart from exposure time) and evaluation procedure as described above. The experimental data were also compared with theoretically predicted structure factor, $S(Q, t)$ from the CHC equation[7,19]

$$S(Q,t) = \frac{RT}{f'' + 2\kappa Q^2} + \left[S_0 - \frac{RT}{f'' + 2\kappa Q^2}\right] \times \exp\left\{-2M(f'' + 2\kappa Q^2)Q^2 t\right\}, \quad (1)$$

where $S_0 = S(Q, t=0)$ is the structure factor of the as-quenched (AQ) material, f'' is the second derivative of the free energy with respect to composition, κ is the gradient energy coefficient, and M is the atomic mobility. Following Marro and Vallés,[25] $S_0 = 1 - x_0^2$, where x_0 is the average Cr content. The peak in the calculated structure factor was evaluated at 773 K for times ranging from 15 min up to 10 h. At 798 K, the predicted second derivative of the molar Gibbs free energy with respect to the mole fraction of Cr is positive, i.e., outside the spinodal, and therefore only calculations at 773 K was performed.

Figure 2 shows the scattering curves obtained directly after reaching the ageing temperature (0 h), as well as after 1 h and after 10 h of ageing at 773 or 798 K. Also included is the as-quenched data recorded at room temperature before heating (AQ RT). The error bars show the statistical error associated with the data acquisition. The increased background at elevated temperatures has been attributed to critical magnetic scattering in the vicinity of the Curie temperature.[10] From Fig. 2, it is clear why the 0 h curve could not be subtracted as background, as the magnitude of the scattering is significantly higher over the entire Q-range

compared to the background in other data sets. The reason for the difference between curves at 0 h and the subsequent acquired data sets is not clear at present. This deviation, as well as the reason for the slowly shifting background, should be further investigated in order to provide a better procedure for background subtraction. Based on the procedure outlined above, the scattering from the spinodal decomposition is shown for selected times in the insets in Fig. 2.

Figure 3 shows the development of the characteristic distance and peak height with ageing time. Both Λ and I_p clearly follows the expected power-law behaviour, with $a' = 0.10$ and 0.11, and $a'' = 0.67$ and 0.86, at 773 and 798 K, respectively. The error bars in Fig. 3(a) represent the estimated drift in the peak position from the temporal averaging over 15 min and is based on the local derivative of the power law fits ($\epsilon_i = \pm \dot{\Lambda}_i \Delta t$, where ϵ_i is the error in data point i, $\dot{\Lambda}_i$ is the derivative of Λ with respect to time at time t_i, and Δt is half the measurement time). This error was found to dominate over the uncertainty in the process of determining Q_p. In Fig. 3(b), the error is based on estimated uncertainty from the fitting of I_b.

The *in-situ* data agree well with the results from *ex-situ* tests of specimens annealed at 773 K. The absolute magnitudes of both Λ and I_p are consistently slightly higher in the *in-situ* experiments, compared to the tests performed *ex-situ*. This could possibly be a result of the background subtraction process, since the shape of the Q-dependent background is different at ambient and elevated temperatures or more likely because the temperatures were not identical during *in-situ* and *ex-situ* ageing. Comparing the 773 and 798 K data, the differences in both peak position and magnitude are much larger than between the *in-situ* and *ex-situ* results. Given that a temperature difference of 25 K has such a large effect, it could be expected that even a small difference in ageing temperature can have an observable impact. This further emphasises the advantage of *in-situ* measurements in order to establish reliable kinetic data, and points to the need of more
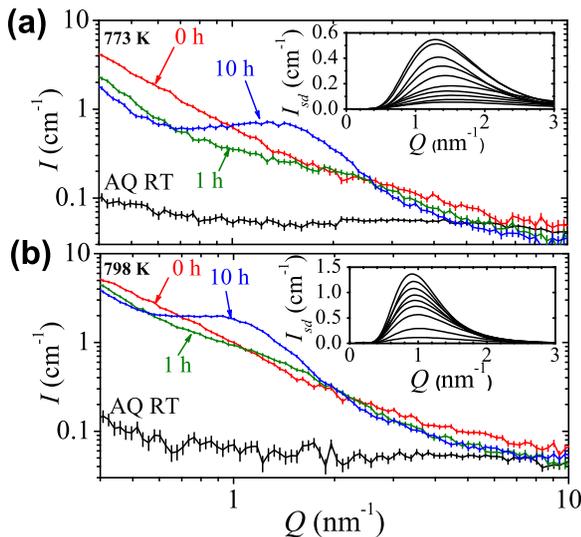

FIG. 2. *In-situ* scattering curves obtained before ageing (AQ RT), directly after heating (0 h) and after 1 and 10 h ageing at (a) 773 and (b) 798 K. The insets show the scattering from the spinodal decomposition, I_{sd}, for selected ageing times.
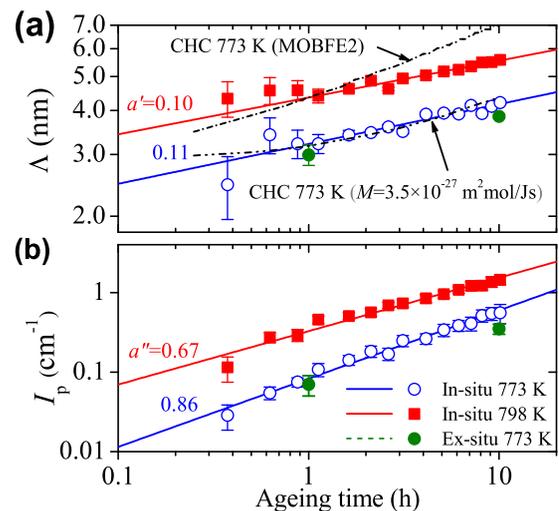

FIG. 3. Time evolution of (a) characteristic distance ($\Lambda = 2\pi/Q_p$) and (b) maximum scattered intensity from the spinodal decomposition ($I_p = d\Sigma/d\Omega(Q_p)$). The black lines show the results from the Cahn-Hilliard-Cook model at 773 K using either mobilities from the *MOBFE2* database or a constant mobility $M = 3.5 \times 10^{-27}\,\text{m}^2\,\text{mol}\,\text{J}^{-1}\,\text{s}^{-1}$.

TABLE I. Comparison of the characteristic distance (in nm) after ageing at 773 K obtained from *in-situ* and *ex-situ* SANS (present investigation) and modulation wavelength from radial distribution function analysis of APT data.[5]

Time (h)	*In-situ*	*Ex-situ*	APT
1	3.2	3.0	…
10	4.2	3.9	3.8

precise thermometry in both *in-situ* and *ex-situ* ageing if values from different tests are to be compared. The value of Λ after 10 h ageing at 773 K also agrees well with the reported modulation wavelength measured by APT,[5] see Table I. The obtained exponents ($a' = 0.10$–0.11, $a'' = 0.67$–0.86) are in the same range as the available literature data,[6–8,10,12,26] although a' is slightly smaller than usually observed. This may be related to the early stages of decomposition studied, since the data presented in, e.g., Ref. 8 show that the slope is smaller at short ageing times (less than 10 h and 1 h at 773 and 798 K, respectively).

It is also highly interesting to compare the *in-situ* data with the CHC theory of spinodal decomposition. The results from the model with $f'' = -261$ J mol^{-1}, $\kappa = 4.07 \times 10^{-16}$ J m^{-2}mol^{-1}, and the mobility calculated from the *MOBFE2* database ($M = x_0 (1 - x_0)(x_0 M_{Fe} + [1 - x_0] M_{Cr}) = 3.49 \times 10^{-26}$ m^2 mol J^{-1}s^{-1}, with $M_{Fe} = 6.4 \times 10^{-26}$ and $M_{Cr} = 2 \times 10^{-25}$ m^2 mol J^{-1}s^{-1}) are included in Fig. 3. The theoretical predictions have a similar behaviour to the experimental data, but the absolute magnitude of Λ is too high, and $a' = 0.20$ is higher than experimentally observed. This disagreement is not unexpected, since the mobilities are highly uncertain at 773 K due to the large extrapolations from higher temperatures. By assuming a lower mobility (in our case $M = 3.5 \times 10^{-27}$ m^{2}mol J^{-1}s^{-1}), good agreement between the CHC predictions and the experimental data is obtained ($a' = 0.12$ and similar magnitudes). It could be noted that the CHC predictions also show a gradually increasing slope with ageing time in the early stages, in agreement with the results in Ref. 8.

Another characteristic feature associated with the progressing decomposition is the slope, n, of the log(I) vs. log(Q) curve beyond Q_p (see Fig. 1(d)). A value of $n = 4$ (Porod's law) indicates sharp interfaces, whereas $n = 2$ is indicative of diffuse compositional fluctuations. In the case of spinodal decomposition, $n = 4$ is usually taken as an indication of a fully developed structure in the coarsening stage. The slope has been used by, e.g., Ujihara and Osamura[8] and Furusaka *et al.*[27] as a means to characterise the development of the decomposition. Figure 4 shows the development of n with ageing time, where an approximate power-law behaviour is observed. During the *in-situ* tests, n increases from around 1 to approximately 2 at 773 K and from 1.5 to slightly below 2.5 at 798 K. The results are consistent with those from the *ex-situ* measurements and indicate that the structure is in the early stages of development after 10 h at the current test temperatures.

Although the present results have been obtained with much higher temporal resolution than previously published
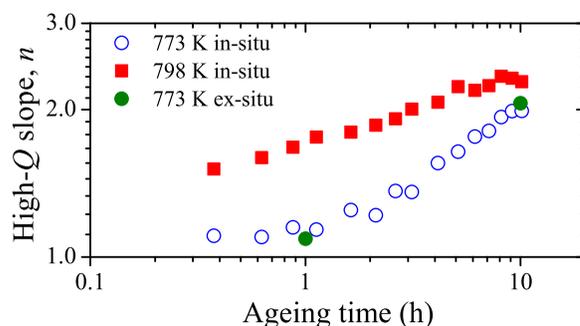

FIG. 4. Change in n, the slope of log(I) vs. log(Q) on the high-Q side of the interference peak, with ageing time.

for the Fe–Cr system, further use of high-flux instruments will enable measurements that can reveal unprecedented details of the early stages of the decomposition. In addition, clarification of the origin of the time-dependent background is necessary in order to improve the procedure for background subtraction. Although the good agreement between the results from the *in-situ* experiments and APT suggests that scattering due to spin-alignment is negligible in the present case, further studies on the effect of external magnetisation are necessary to quantify the magnetic scattering contribution.

In summary, the present work reports the time-resolved *in-situ* investigation of the early stages of spinodal decomposition in the Fe–Cr system. The results show that both the characteristic distance and intensity at 773 and 798 K follow a power-law behaviour, and the evolution at 773 K is in good agreement with theoretical predictions from the Cahn-Hilliard-Cook model with constant mobility. Furthermore, the method allows tracking of the high-Q slope, which is a sensitive measure of the early stages of decomposition.

[1]P. Hedström, S. Baghsheikhi, P. Liu, and J. Odqvist, Mater. Sci. Eng. A **534**, 552 (2012).
[2]D. Chandra and L. Schwartz, Metall. Trans. **2**, 511 (1971).
[3]J. Cislak, S. Dubiel, and B. Sepiol, J. Phys.: Condens. Matter **12**, 6709 (2000).
[4]M. Miller, J. Hyde, M. Hetherington, A. Cerezo, G. Smith, and C. Elliott, Acta Metall. Mater. **43**, 3385 (1995).
[5]J. Zhou, J. Odqvist, M. Thuvander, and P. Hedström, Microsc. Microanal. **19**, 665 (2013).
[6]F. Bley, Acta Metall. Mater. **40**, 1505 (1992).
[7]J. LaSalle and L. Schwartz, Acta Metall. **34**, 989 (1986).
[8]T. Ujihara and K. Osamura, Acta Mater. **48**, 1629 (2000).
[9]K. Hawick, J. Epperson, C. Windsor, and V. Rainey, *Proceedings of the Materials Research Society Fall Meeting, Nov.-Dec. 1990* (Mater. Res. Soc. Symp. Proc., 1990).
[10]J. Epperson, V. Rainey, C. Windsor, K. Hawick, and H. Chen, *Proceedings of the Materials Research Society Fall Meeting, Nov.-Dec. 1990* (Mater. Res. Soc. Symp. Proc., 1990).
[11]E. Eidenberger, M. Schober, P. Staron, D. Caliskanoglu, H. Leitner, and H. Clemens, Intermetallics **18**, 2128 (2010).

[12]M. Furusaka, Y. Ishikawa, S. Yamaguchi, and Y. Fujino, J. Phys. Soc. Jpn. **55**, 2253 (1986).

[13]W. Xiong, P. Hedström, M. Selleby, J. Odqvist, M. Thuvander, and Q. Chen, CALPHAD **35**, 355 (2011).

[14]Y. Wang, R. Kampmann, and R. Wagner, Physica B **234–236**, 992 (1997).

[15]K. Binder and D. Stauffer, Phys. Rev. Lett. **33**, 1006 (1974).

[16]J. Marro, A. Bortz, M. Kalos, and J. Lebowitz, Phys. Rev. B **12**, 2000 (1975).

[17]J. Marro, J. Lebowitz, and M. Kalos, Phys. Rev. Lett. **43**, 282 (1979).

[18]P. Hedström, F. Huyan, J. Zhou, S. Wessman, M. Thuvander, and J. Odqvist, Mater. Sci. Eng. A **574**, 123 (2013).

[19]H. Cook, Acta Metall. **18**, 297 (1970).

[20]R. Heenan, J. Penfold, and S. King, J. Appl. Cryst. **30**, 1140 (1997).

[21]See http://www.mantidproject.org for the Mantid project, with information, documentation, and software download.

[22]G. D. Wignall and F. S. Bates, J. Appl. Cryst. **20**, 28 (1987).

[23]A. Michels and J. Weissmüller, Rep. Prog. Phys. **71**, 066501 (2008).

[24]A. Isalgué, M. Anglada, J. Rodriquez-Carvajal, and A. de Geyer, J. Mater. Sci. **25**, 4977 (1990).

[25]J. Marro and J. Valles, Phys. Lett. A **95**, 443 (1983).

[26]S. Katano and M. Iizumi, Physica B **120**, 392 (1983).

[27]M. Furusaka, Y. Ishikawa, and M. Mera, Phys. Rev. Lett. **54**, 2611 (1985).